Meet Am Soc Stereotact Funct Neurosurg, Snowbird, Utah, 1999
Stereotact Funct Neurosurg 1999;73:50–59

Stereotactic and Functional Neurosurgery

# Stereotactic Radiosurgery of Cerebral Arteriovenous Malformations: Appearance of Perinidal $T_2$ Hyperintensity Signal as a Predictor of Favorable Treatment Response

Fardad Mobin[b] Antonio A.F. De Salles[a] Osama Abdelaziz[c]
Cynthia Cabatan-Awang[a] Timothy Solberg[a] Michael Selch[a]

[a]Department of Neurosurgery and Radiation Oncology, School of Medicine, University of California, Los Angeles, Calif., and [b]University of California, Davis, Calif., USA; [c]Department of Neurosurgery, Alexandria University, Alexandria, Egypt

Key Words
Stereotactic radiosurgery · Arteriovenous malformations · Magnetic resonance imaging · Treatment response · Stereotactic surgery

Abstract

The purpose of this study was to analyze the significance of perinidal $T_2$ hyperintensity appearance after radiosurgery of arteriovenous malformations (AVMs), as a predictor of treatment response. Our initial experience with linear accelerator (LINAC) radiosurgery at University of California, Los Angeles, between 1990 and 1997 involved treatment of 129 patients affected by cerebral AVMs. Based upon availability of neuroimaging follow-up, 48 patients with 50 AVMs were selected for review. Forty (80%) of the AVMs underwent complete obliteration or significant reduction on follow-up MRI, on average 20 months after radiosurgery. Thirteen (72%) of 18 obliterated AVMs were associated with perinidal $T_2$ hyperintensity signal, on average 18 months (6–49) after radiosurgery. Ten (20%) of 50 AVMs (average volume 23.1 $cm^3$, ranging 7.5–46.5) were unchanged. Furthermore, only

KARGER
Fax + 41 61 306 12 34
E-Mail karger@karger.ch
www.karger.com


1011–6125/99/0734–0050$17.50/0

Accessible online at:
www.karger.com/journals/sfn

Dr. Fardad Mobin, Neurological Surgery
University of California, 4860 Y Street, Suite 3740
Sacramento, CA 95817 (USA)
Tel. +1 916 734 3658, Fax +1 916 734 3232
E-Mail fmobin@pol.net

3 AVMs in this group showed reversible $T_2$ signal changes. In patients with complete nidal obliteration, appearance of $T_2$ hyperintensity signal achieves 72% sensitivity in predicting successful treatment response.



## Introduction

Cerebral arteriovenous malformations (AVMs) are believed to be congenital or acquired arterial-to-venous shunts that lack intervening capillary network [1–3]. The AVM nidus is composed of tangled arterioles admixed with gliotic parenchyma, shunting arterialized blood to the draining veins. Depending on size, hemodynamic factors, number of feeding vessels, pattern of venous drainage and presence of flow-related or nidal aneurysms, AVMs may present with intracerebral hemorrhage, seizures, neurologic deficit, headaches or occasionally as incidental findings on neuroimaging studies [4–10]. Several studies on the natural history of AVMs have captured the high propensity of these lesions to hemorrhage at the first presentation [11–14], each event carrying 1% mortality and 2–4% major morbidity per year. The goal of treatment should be complete AVM nidal obliteration while preserving the normal functioning of the adjacent brain parenchyma and providing the patient with a reasonable margin of therapeutic safety as compared to the natural history of the disease. To this end, stereotactic radiosurgery has provided an elegant means of safely treating arteriovenous malformations, including those recognized by the Spetzler-Martin grading system as 'high-grade' [15–19]. The most significant shortcoming of radiosurgical therapy of cerebral AVMs is the prolonged time interval superseding actual nidal obliteration which may last from 6 months to several years [20–22]. The persistent chance of hemorrhage from the partially obliterated nidus during the latency period mandates diligent neuroimaging follow-up of the radiosurgical patient until proven nidal obliteration. Magnetic resonance imaging (MRI) has offered an accurate, noninvasive modality for evaluation of AVM patency, as well as providing information regarding the changes in the surrounding brain parenchyma after radiosurgery [23–26]. The aim of this paper is to evaluate the postradiosurgical MRI changes, specifically the appearance of perinidal $T_2$ hyperintensity as a predictor of eventual AVM response to radiosurgical treatment.

## Patients and Methods

Our initial experience with linear accelerator (LINAC) radiosurgery at University of California, Los Angeles, between 1990 and 1997, involved treatment of 129 patients affected by cerebral AVMs. Patient referral was based either on 'inoperability' or refusal of

Table 1. Clinical characteristics of 48 radiosurgical patients with AVMs

| Factor | Cases | |
|---|---|---|
| | n | % |
| *Sex* | | |
| Male | 23 | 47 |
| Female | 25 | 53 |
| *Location* | | |
| Cerebral lobe | 34 | 69 |
| Thalamus | 5 | 11 |
| Basal ganglia | 3 | 6 |
| Pons/midbrain | 3 | 6 |
| Cerebellum | 4 | 6 |
| Corpus callosum | 1 | 2 |
| *Spetzler-Martin* | | |
| I | 0 | 0 |
| II | 6 | 12 |
| III | 11 | 22 |
| IV | 12 | 24 |
| V | 19 | 38 |
| VI | 2 | 4 |

open surgery. Forty-eight patients with 50 AVMs were retrospectively chosen based upon availability of neuroimaging follow-up. Clinical characteristics of this patient population are summarized in table 1. At the time of radiosurgery, the patients' age ranged from 9 to 76 with a mean of 38.3 years.

*Localization of the AVM*

All patients underwent placement of a BRW frame (Brown, Robert, Wells; Radionics Inc., Burlington, Mass., USA) and an appropriate fiducial box prior to biplane stereotactic angiography, contrast CT and MRI scanning. Stereotactic angiography images were digitally scanned into the radiosurgical planning software, using either the Philips SRS200 (Philips Medical Systems, Shelton, UK), or the X-Knife system (Radionics Inc.). The scanned images were then registered with the corresponding CT images and imported electronically. In cases pretreated with radio-opaque embolic material, MRI images proved especially helpful in defining the AVM nidus.

*Radiosurgical Technique*

With the aid of an image-integrated computer planning system, single-dose treatment plans achieved full nidus coverage in all patients. Four to eight noncoplanar converging arcs of radiation were used for each isocenter. Beam diameter varied from 7 to 52.5 mm (mean 26.6). Nine (18%) of 50 AVMs were less than 4 $cm^3$ in volume, treated with one isocenter, an average prescribed dose of 17.6 Gy (range 14–25) to an average isodose line of 84% (range

80–90%). Eleven (22%) AVMs measured 4–10 $cm^3$ in size (average 6.3) were treated with one isocenter, with an average prescribed dose of 16.2 Gy (range 13–22), to the average isodose line of 81.4% (range 50–90%). The remaining 29 (58%) AVMs were >10 $cm^3$, averaging 31.3 $cm^3$ in size, were treated with 1–2 isocenters, with an average prescribed dose of 14 Gy (range 12–18), to the average isodose line of 80% (range 50–90%).

*Preradiosurgical Embolization*

Eighteen (36%) of 50 AVMs were embolized prior to radiosurgery. Embolization was performed in stages for large-sized AVMs to prevent normal pressure perfusion breakthrough and optimize patient tolerance. Flow-directed microcatheters were used to deliver embolic material or electrically detachable platinum coils (GDC coils) to obliterate intranidal fistulae or associated proximal aneurysms. Volume changes were obtained from pre- and postembolization angiograms. Of the embolized patients, 22.2% underwent stereotactic radiosurgery within 1 week, 39% within 3 months, 16.8% within 6 months and 22% more than 6 months following embolization.

*Imaging Follow-Up*

A 1.5-tesla MRI system (Signa; General Electric Corp., Milwaukee, Wisc., USA) was used in all cases. Spin-echo pulse sequence $T_1$-weighted (TR 533 ms/TE 14 ms) and fast spin-echo $T_2$-weighted (TR 3,100 ms/TE 84 ms) coronal and axial images were obtained. Slice thickness was 5.0 mm, and the interslice gap was 1.5 mm, covering the entire brain. The field of view was 18 × 18 and a 256 × 256 matrix was used. The first MRI scan was obtained 3 months after treatment, followed by scans at 6-month intervals, until MRI evidence of nidal obliteration. Then, a confirmatory cerebral angiogram was obtained in compliant patients. Generally, a follow-up period of 3 years was observed before decision to repeat stereotactic radiosurgery in patients with persistent AVM nidus. Patients with magnetic resonance images significant for reversible perilesional $T_2$ signal were selected for review. MRI in 3 patients in addition to reversible perinidal $T_2$ change demonstrated perinidal parenchymal enhancement on $T_1$-weighted images after administration of gadolinium.

## Results

MRI follow-up revealed 40 (80%) of the 50 AVMs to have a significant reduction in volume or complete nidal obliteration on average 20 months after radiosurgery. Of the AVMs with MRI evidence of postradiosurgical reduction or obliteration, 18 (45%) had angiographically proven nidal obliteration. Thirteen (72%) of 18 obliterated AVMs were associated with perinidal $T_2$ hyperintensity signal on average 18 months (6–49) after radiosurgery. Three (25%) of the 13 AVMs showed evidence of encephalomalacia and radiation necrosis, evidenced by gadolinium enhancement in the surrounding white matter. Ten (20%) of the 50 AVMs were unchanged after radiosurgery (average volume 23.1 $cm^3$, range 7.5–46.5). Furthermore, only 3 (30%) AVMs in this group showed reversible $T_2$ signal changes after radiosurgery. Figure 1 is a summary of the results comparing

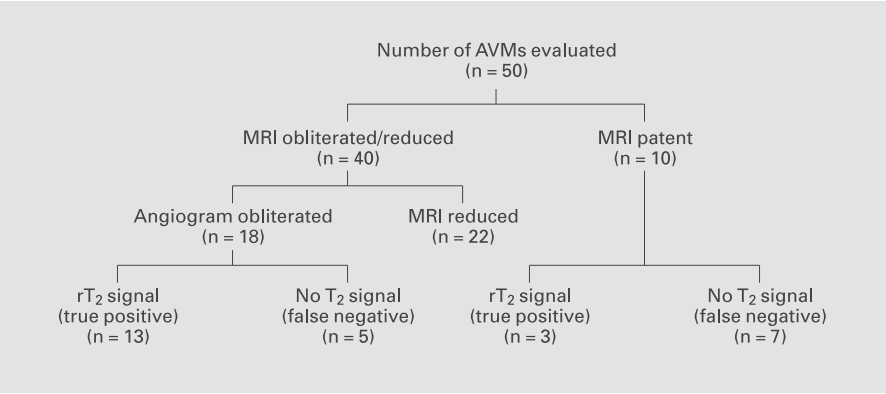


Fig. 1. Diagram comparing the distribution of MRI perinidal $T_2$ appearance in the angiographically obliterated subset of AVMs and MRI-patent AVMs. $rT_2$ = reversible $T_2$ signal.

Table 2. Comparison of the MRI perinidal $T_2$ signal appearance in angiographically obliterated AVMs and MRI-patent AVMs

| Characteristics | Results |
|---|---|
| Sensitivity of $T_2$ appearance for obliteration | 13/18 (72) |
| Specificity of $T_2$ appearance for obliteration | 7/10 (70) |
| False-negative rate | 5/18 (28) |
| False-positive rate | 3/10 (30) |
| Positive predictive value | 13/18 (72) |
| Negative predictive value | 7/10 (70) |
| Overall accuracy | 20/28 (71) |

Figures in parentheses are percentages.

sensitivity and specificity of perinidal $T_2$ appearance on MRI as a predictor of angiographic obliteration. Comparisons between the subset of AVMs with proven angiographical obliteration and MRI-patent AVMs, with regard to the appearance of perinidal $T_2$ signal, are listed in table 2. Appearance of the $T_2$ hyperintensity signal had a 72% sensitivity and 70% specificity in predicting successful treatment response.

## Discussion

Ionizing radiation delivered stereotactically to the AVM nidus produces a cascade of reactions culminating in eventual nidal obliteration [27]. The evolution of changes that lead to the obliteration of the AVM begin with the acute-phase response, including endothelial cell swelling, opening of the tight junctions between the endothelial cells and eventual breakdown of the blood-brain barrier. The acute-phase response is thought to contribute to the genesis of the high $T_2$ signal in form of steroid-responsive vasogenic edema secondary to transudate formation [28]. On the other hand, the chronic phase of radiation-induced changes is characterized by intimal and adventitial proliferation and hyalin degeneration of the vasculature [28–30]. Endothelial cell hyperplasia and intimal thickening leading to progressive luminal occlusion and thrombosis have been described in animal models of radiosurgery [27, 31, 32]. Szeifert et al. [33] and others [34, 35] have described irradiation-induced changes in surgical and autopsy specimen of AVM nidus, including subendothelial stromal changes, notably myofibroblast proliferation, deposition of collagen type IV fibers and focal calcification leading to scar tissue formation and contraction of the thrombosed AVM nidus. Yamamoto et al. [36] have reported a spectrum of changes in the nidus-unrelated arteries, from fragmentation of the elastic laminae to intimal hypertrophy and complete luminal occlusion in vessels exposed to 10–25 Gy.

There are several neuroimaging modalities, such as CT, positron emission tomography, MRI and the gold standard cerebral angiography, which allow the clinician to monitor obliteration of the irradiated AVM. MRI has been increasingly utilized to help evaluate postradiosurgical patients, due to its noninvasiveness and lack of ionizing radiation exposure. MRI lends itself particularly to evaluation of acute- as well as chronic-phase changes described above.

Our hypothesis regarding the appearance of perinidal $T_2$ signal changes in association with nidal obliteration is based upon the assumption that irradiation-induced changes have variable effects on nidal and perinidal vessels. The differential response of the endothelial cells is an epiphenomenon resulting from the spatial distribution of irradiation dosimetry. Nidal vessels, which experience greater radiation dosage because of proximity to the isocenter, will go on to occlude as compared to the perinidal vessels, which by virtue of greater displacement from the isocenter undergo fragmentation of the elastic laminae and hyalinization of the periadventitia with subsequent increased permeability (fig. 2).

An explanation for the appearance of the reversible perinidal $T_2$ hyperintensity signal, consistent with vasogenic edema, could be rendered in terms of the evolution of hemodynamic changes in the irradiated AVM nidus. As the cascade of nidal involution progresses, the intranidal blood flow diminishes with subsequent rise of hydrostatic pressure in the prenidal vessels. Increased intraluminal

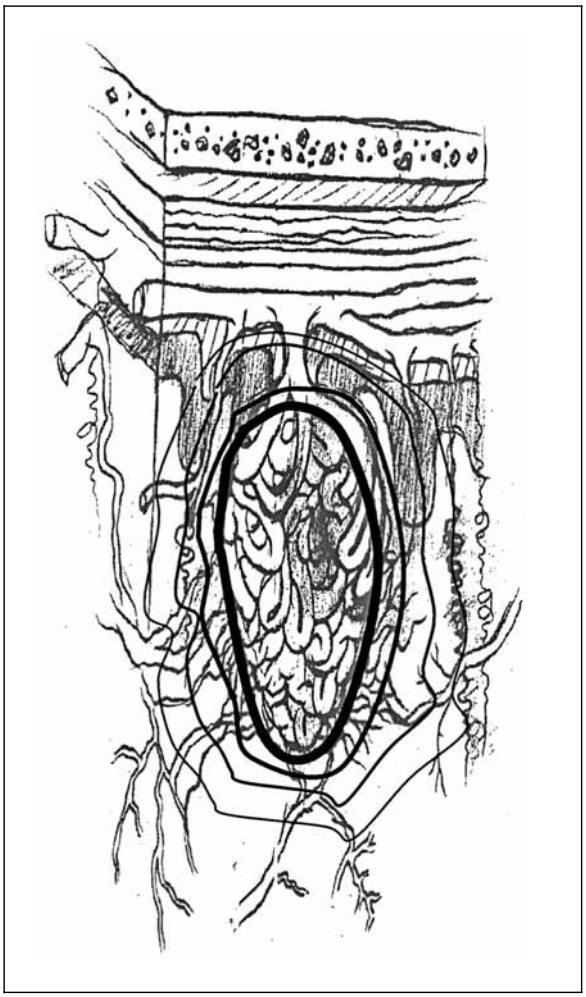

Fig. 2. A representation of an isodose plan for an AVM nidus. From the center of the nidus, isodose lines are at 90, 70, 50 and 30%, respectively. Irradiating the nidus at 18 Gy to the 90% isodose line exposes the perinidal arterioles within the 70 and 50% isodose lines from 9 to 12.6 Gy.

hydrostatic pressure in the prearteriolar vessels experiencing partial irradiation-induced damage would then become the principal mechanism responsible for $T_2$ signal appearance. Transudation of plasma proteins and the increased hydrostatic pressure in the prenidal arterioles obeying Starling forces would favor transluminal fluid efflux and subsequent formation of perinidal edema. In this setting,

perinidal edema formation would be an indicator of nidal response to radiosurgical therapy. Furthermore, greater radiation-exposure to perinidal vessels would theoretically generate a greater potential for edema formation, in proportion to the AVM size and treatment dose [28]. Further understanding of the regional variables, such as the degree of perinidal loss of autoregulatory function, perfusion-metabolism mismatch in the surrounding parenchyma, venous hypertension and, more importantly, the hemodynamic profile of the AVM may serve in the future for improved predictability of postradiosurgical behavior of the nidus.

The fact that the hemorrhage rate during the latency period after the radiosurgical treatment of the AVM nidus is not increased compared to the rate of bleeding expected from the natural history studies [20–22] could be accounted for by the differential effect of the radiation on the nidal vessels; namely arteriolar thrombosis more prevalent and prior to venous changes and secondly diminished intraluminal pressure from the prearteriolar vessels in form of perinidal edema.

The dramatic fall in the intranidal blood flow during nidal obliteration parallels the fall in the intraluminal hydrostatic pressure of the prenidal arterioles. With loss of the pressure gradient across these vessels, the rate of perinidal fluid formation would in turn fall with eventual resolution of the perinidal $T_2$ hyperintensity signal. In the majority of our patients, resolution of perinidal $T_2$ hyperintensity signal was observed over 5–18 months from the time of onset. In symptomatic patients, steroids and occasionally rheologic agents such as pentoxifylline (Trental®) were used to catalyze the resolution of the edema.

Other investigators have also reported an occurrence of perinidal high $T_2$ MRI signal after stereotactic radiosurgery of AVMs with histopathological correlates of blood-brain barrier breakdown, interstitial vasogenic edema and reactive astrogliosis [32, 37, 38]. Lunsford et al. [38] have classified postradiosurgical MRI findings with respect to nidal and perinidal reactions, finding a greater association of perilesional $T_2$ hyperintensity signal after the treatment of AVMs as compared to the other intracranial lesions in their series.

In those patients with persistent although smaller regions of increased $T_2$ signal, other mechanisms such as perinidal gliosis, irradiation-induced angiogenesis and blood product deposition may be responsible. These other mechanisms can be distinguished from the perinidal $T_2$ hyperintensity secondary to vasogenic processes explained above by studying the MRI characteristics of the lesion with respect to its $T_1$ appearance, pattern of gadolinium enhancement and the reversibility of the lesion.

## References


1 McCormick WF: Pathology of the vascular malformations of the brain; in Wilson CB, Stein BM (eds): Intracranial Arteriovenous Malformations. Baltimore, Williams and Wilkins, 1984, pp 44–65.
2 Marin-Padilla M: Embryology; in Yasargil MG (ed): AVM of the Brain: History, Embryology, Pathological Considerations, Hemodynamics, Diagnostic Studies, Microsurgical Anatomy, in Microneurosurgery: IIIA. Stuttgart, Thieme, 1987, pp 23–47.
3 Nussbaum ES, Heros RC, Madison MT, Awasthi D, Truwit C: The pathogenesis of arteriovenous shunts: Insights provided by a case of multiple arteriovenous malformations developing in relation to a developmental venous anomaly concept. Neurosurgery 1998;43:347–352.
4 Perret G, Nishioka H: Report on the Cooperative Study of Intracranial Aneurysms and Subarachnoid Hemorrhage. Section VI. Arteriovenous malformations. An analysis of 545 cases of craniocerebral arteriovenous malformations and fistulae reported by the Cooperative Study. J Neurosurg 1966;25:467–490.
5 Manchola IF, De Salles AAF, Foo TK, Ackerman RH, Candia GT, Kjellberg RN: Arteriovenous malformations hemodynamics: A transcranial Doppler study. Neurosurgery 1993;33:556–562.
6 Spetzler RF, Hargraves RW, McCormick PW, Zabramski JM, Flom RA, Zimmerman RS: Relationship of perfusion pressure and size to risk of hemorrhage from arteriovenous malformation. J Neurosurg 1992;76:918–923.
7 Langer DJ, Lasner TM, Hurst RW, Flamm ES, Zager EL, King JT Jr: Hypertension, small size, and deep venous drainage are associated with risk of hemorrhagic presentation of cerebral arteriovenous malformations. Neurosurgery 1998;42:481–486.
8 Miyasaka Y, Yada K, Ohwada T, Kitahara T, Kurata A, Irikura K: An analysis of the venous drainage system as a factor in hemorrhage from arteriovenous malformations. J Neurosurg 1992; 76:239–243.
9 Thompson RC, Steinberg GK, Levy RP, Marks MP: The management of patients with arteriovenous malformations and associated intracranial aneurysms. Neurosurgery 1998;43:202–211.
10 Perata HJ, Tomsick TA, Tew JM Jr: Feeding artery pedicle aneurysms: Association with parenchymal hemorrhage and arteriovenous malformation in the brain. J Neurosurg 1994;80:631–634.
11 Fults D, Kelly DL: Natural history of arteriovenous malformations of the brain: A clinical study. Neurosurgery 1984;15:658–662.
12 Ondra SL, Troupp H, George ED, Schwab K: The natural history of symptomatic arteriovenous malformations of the brain: A 24-year follow-up assessment. J Neurosurg 1990;73:387–391.
13 Brown RD Jr, Wiebers DO, Forbes G, O'Fallon WM, Piepgras DG, Marsh WR, Maciunas RJ: The natural history of unruptured intracranial arteriovenous malformations. J Neurosurg 1998;68:352–357.
14 Graf CJ, Perret GE, Torner JC: Bleeding from cerebral arteriovenous malformation as part of their natural history. J Neurosurg 1983;58:331–337.
15 Spetzler RF, Martin NA: A proposed grading system for arteriovenous malformations. J Neurosurg 1986;65:476–483.
16 Colombo F, Pozza F, Chierego G, Casentini L, De Luca G, Francescon P: Linear accelerator radiosurgery of cerebral arteriovenous malformations: An update clinical study. Neurosurgery 1994;34: 14–21.
17 Pollock BE, Lunsford LD, Kondziolka D, Maitz A, Flickinger JC: Patient outcome after stereotactic radiosurgery for 'operable' arteriovenous malformations. Neurosurgery 1994;35:1–8.
18 Lindquist C, Steiner L: Stereotactic radiosurgical treatment of malformations of the brain; in Lunsford LD (ed): Modern Stereotactic Neurosurgery. Boston, Nijhoff, 1988, pp 491–506.
19 Friedman WA, Bova FJ: Radiosurgery for arteriovenous malformations; in Youmans J (ed): Neurological Surgery. Philadelphia, Saunders, 1996, Ch 60.
20 Pollock BE, Flickinger JC, Lunsford LD, Bissonette DJ, Kondziolka D: Hemorrhage risk after stereotactic radiosurgery of cerebral arteriovenous malformations. Neurosurgery 1996;38:652–659.
21 Karlsson B, Lindquist C, Steiner L: Effect of Gamma knife surgery on the risk of rupture prior to AVM obliteration. Minim Invas Neurosurg 1996;39:21–27.

22 Friedman WA, Blatt DL, Bova FJ, Buatti JM, Mendenhall WM, Kubilis PS: The risk of hemorrhage after radiosurgery for arteriovenous malformations. J Neurosurg 1996;84:912–919.
23 Flickinger JC, Lunsford LD, Kondziolka D, Maitz AH, Epstein AH, Simons SR, Wu A: Radiosurgery and brain tolerance: An analysis of neurodiagnostic imaging changes after gamma knife radiosurgery for arteriovenous malformations. Int J Radiat Oncol Biol Phys 1992;23:19–26.
24 Kihlstrom L, Guo WY, Karlsson B, Lindquist C, Lindqvist M: Magnetic resonance imaging of obliterated arteriovenous malformations up to 23 years after radiosurgery. J Neurosurg 1997;86: 589–593.
25 Pollock BE, Kondziolka D, Flickinger JC, Patel AK, Bissonette DJ, Lunsford LD: Magnetic resonance imaging: An accurate method to evaluate arteriovenous malformations after stereotactic radiosurgery. J Neurosurg 1996;85:1044–1049.
26 Yananoto M, Ide M, Jimbo M, Takakura K, Lindquist, Steiner L: Neuroimaging studies of postobliteration nidus changes in cerebral arteriovenous malformations treated by gamma knife radiosurgery. Radiosurgery 1996;45:110–122.
27 De Salles AAF, Solberg T, Mischel P, et al: Arteriovenous malformation animal model for radiosurgery: The rete mirabile. Am J Neuroradiol 1996;17:1451–1458.
28 Kjellberg RN, Hanamura T, Davis KR, Lyons SL, Adams RD: Bragg-peak proton-beam therapy for arteriovenous malformations of the brain. N Engl J Med 1983; 309:269–274.
29 Kjellberg RN: Proton beam therapy for arteriovenous malformations of the brain; in Schmidek HH, Sweet WH (eds): Operative Neurosurgical Techniques: Indications, Methods, and Results. Philadelphia, Saunders, 1988, pp 911–915.
30 Martins AN, Johnston JS, Henry JM, Stoffel TJ, Chiro GD: Delayed radiation necrosis of the brain. J Neurosurg 1977;47:336–345.
31 Blatt DR, Friedman WA, Bova KJ, Theele DP, Mickle JP: Temporal characteristics of radiosurgical lesions in an animal model. Neurosurgery 1994;80:1046–1055.
32 Lunsford LD, Kondziolka D, Flickinger JC, Bissonette DJ, Jungreis CA, Maitz AH, Horton JA, Coffey RJ: Stereotactic radiosurery for arteriovenous malformations of the brain. J Neurosurg 1991;75:512–524.
33 Szeifert GT, Kemeny AA, Timperley WR, Forster DMC: The potential role of myofibroblasts in the obliteration of arteriovenous malformations after radiosurgery. Neurosurgery 1997;40:61–66.
34 Steinberg GK, Chang SD, Levy RP, Marks MP, Frankel K, Marcellus M: Surgical resection of large incompletely treated intracranial arteriovenous malformations following stereotactic radiosurgery. J Neurosurg 1996;84:920–928.
35 Schneider BF, Eberhard DA, Steiner LE: Histopathology of arteriovenous malformations after gamma knife radiosurgery. J Neurosurg 1997;87:352–357.
36 Yamamato M, Jimbo M, Ide M, Kobayashi M, Toyoda C, Lindquist C, Karlson B: Gamma knife radiosurgery for cerebral arteriovenous malformations: An autopsy report focusing on irradiation-induced changes observed in nidus-unrelated arteries. Surg Neurol 1995;44:421–427.
37 Adams RD: The neuropathology of radiosurgery. Stereotact Funct Neurosurg 1991;57:82–86.
38 Lunsford LD, Kondziolka D, Maitz A, Flickinger JC: Black holes, white dwarfs and supernovas: Imaging after radiosurgery. Stereotact Funct Neurosurg 1998;70(suppl 1):2–10.